

New 3-bar prismatic tensegrity units

Heping Liu^{a,c*}, Jingyao Zhang^b and Makoto Ohsaki^a

^a Department of Architecture and Architectural Engineering, Kyoto University, Kyoto-Daigaku Katsura, Nishikyo, Kyoto 615-8540, Japan

^b Department of Architecture and Urban Design, Nagoya City University, Chikusa-ku, Nagoya, 464-0083, Japan

^c College of Mechanical and Electrical Engineering, Harbin Engineering University, Harbin 150001, China

*Corresponding author. E-mail address: liuheping1234@sohu.com

This study was carried out during the first author's stay at Kyoto University.

Abstract: Various methods have been presented for generating complex tensegrity structures by assembling simple units. Hence, generating new units will in turn benefit in obtaining various shapes of tensegrity structures. In this paper, we present three different new units by adding strings to the well-known 3-bar prismatic tensegrity unit. Analytical solutions are derived for their self-equilibrium analysis. Influences of structural parameters on internal forces of the members are investigated to study properties of the new tensegrity units.

Keywords: tensegrity unit; additional nodes and strings; self-equilibrium; prismatic unit.

1 Introduction

A tensegrity structure is composed of strings and bars [1]. In the strict definition of tensegrity structure, its rigid bars do not touch with each other, and are connected with strings [2]. All members of a tensegrity structure bear only axial forces [3]. Since a tensegrity structure with sparse members is statically indeterminate, self-equilibrium forces exist in the structure, it can bear large external forces and own light weight.

Tensegrity structures have many applications in different areas [4]. For example, when it is used for a planetary landing device, its continuous string net on the surface can support and protect bars inside it, and the net can absorb external shocks owing to its flexibility [5]. The above unique characteristics have made the tensegrity structures become a research hotspot.

Tensegrity units are the bases of some complex tensegrity structures. The needle tower built by Snelson in 1968 is a tensegrity structure consisting of axially connected several 3-bar tensegrity units [6]. The ball tensegrity robots by NASA are built with two 3-bar tensegrity units [7-9]. Caluwaerts and Carbajal [10] built a 12-bar tensegrity stacked by three 4-bar tensegrity units. Liu *et al.* [11] analyzed the tensegrity connecting units along its axis. Luo *et al.* [12] constructed the spherical tensegrity structure with several tensegrity units. Therefore, developing new configurations of the tensegrity units will help obtain more various types of tensegrity structures.

Determination of self-equilibrium state is always a key point of research on shape design of tensegrity structures. In the self-equilibrium analysis, equilibrium matrix is formulated in various forms and investigated using various tools. Pellegrino [13] used singular value

decomposition (SVD) of the equilibrium matrix to analyze a static, kinematic, or static/kinematic nature of any structural assembly. In his analysis, numbers of independent zero-energy deformation modes and independent states of self-stress were computed to classify the structures. Zhang *et al.* [14] decomposed the equilibrium matrix to compute the independent states of self-stress. An optimization method for the purpose of maximizing the global rigidity of the structure is applied to determine the combination coefficients of the independent symmetric self-stress states. Xu *et al.* [15] obtained the independent states of self-stresses and internal mechanisms of tensegrity structures by applying SVD to numerical expression of the equilibrium matrix. The method based on simulated annealing was adopted to further find a feasible state of self-stresses. Through comparison of dimension of the structure with rank deficiency of the equilibrium equations with respect to nodal coordinates, Zhang *et al.* [16] presented the necessary conditions for guaranteeing that a free-standing prestressed structure is non-degenerate.

Prestressed tensegrity structures must satisfy equilibrium equations defined by structural parameters, which conversely means that the equilibrium equations characterize the properties of structural parameters. Moreover analytical solutions, rather than numerical ones, of structural parameters can reflect relations between the parameters. Tibert and Pellegrino [17] solved equilibrium equations in symbolic form to obtain easily equilibrium conditions of the well-known prismatic tensegrity units.

In this paper, we present several new configurations for tensegrity units by adding strings to the existing 3-bar prismatic tensegrity units. Equilibrium equations are solved in symbolic form to obtain analytical solutions of structural parameters, aiming at finding general characteristics of the new tensegrity structures studied in this paper.

2 Definition of prismatic tensegrity unit

We consider a 3-bar prismatic tensegrity unit as shown in Fig.1(a). The thick lines in the figure are bars carrying compression and the thin lines refer to strings carrying tension. All members of the structure can be classified into four kinds: bars, declining strings, upper level strings, and lower level strings. Equilibrium of the tensegrity unit is dependent on α ($\alpha \in [-180^\circ, 180^\circ]$), which is the angle projected on the lower plane and rotated from node 1 to node 4 as shown in Fig. 1(a). Note here that nodes 1 and 4 are connected by a bar.

When the 3-bar tensegrity unit is at self-equilibrium state, the angle α must satisfy [18]

$$\alpha = \pm 150^\circ \quad (1)$$

Two 3-bar tensegrity units corresponding to $\alpha=150^\circ$ and -150° are distinguished by the connectivity of declining strings. Figure 1(a) shows the case of $\alpha=150^\circ$, where nodes 1, 2 and 3 are connected to nodes 6, 4 and 5, respectively, by the declining strings. By contrast, when $\alpha=-150^\circ$, nodes 1, 2 and 3 are connected to nodes 5, 6 and 4, respectively. Zhang *et al.* [19] showed that strings can be added between the existing nodes, as shown with dotted lines in Fig.1(b), to make the 3-bar tensegrity units at equilibrium with α in the range of $[-180^\circ, -150^\circ] \cup [150^\circ, 180^\circ]$.

In this paper, we use the structure in Fig.1(a) as the base structure. A node is added to each upper level string, and the additional nodes are connected to the nodes on the lower

plane by the additional strings.

3 New configurations by addition of members

To generate new units, every string on the upper plane of the 3-bar prismatic structure in Fig. 1(a) is split into two strings, called *first and second upper level strings*, by the additional node. Moreover, there are three different cases for connectivity of an additional string connecting the additional node to an existing node on the lower plane, as shown in Fig. 2. For each additional node, there are three strings connecting it to the existing nodes, and therefore, these three strings and the four nodes connected to the additional node have to be on the same plane to satisfy self-equilibrium. Accordingly, topology of the unit is classified into three types by the group of four nodes as listed in Table 1, where $\{i, j, k, l\}$ ($i, j, k, l \in \{1, \dots, 9\}$) indicates the nodes i, j, k and l are on the same plane.

If there exists a structure at self-equilibrium for a specified value of $\alpha = \alpha^*$, it is easily seen from symmetry property that there exists another configuration corresponding to $\alpha = -\alpha^*$.

Therefore, we investigate mainly the structure with $\alpha \in [0^\circ, 180^\circ]$.

Let r_1 and r_2 denote radii of the circles containing the existing nodes respectively on the upper and lower planes as shown in Fig.1(b). Height of the 3-bar unit is denoted by H . Let N_i ($i=1, \dots, 9$) denote coordinate vector of the i th node. Coordinates of the nodes located on the lower plane can be written as

$$N_k = \begin{bmatrix} r_1 \cos[2\pi(k-1)/3] \\ r_1 \sin[2\pi(k-1)/3] \\ 0 \end{bmatrix} \quad (k=1, 2, 3) \quad (2)$$

Nodal coordinates on the upper plane can be written as

$$N_k = \begin{bmatrix} r_2 \cos[2\pi(k-4)/3 + \alpha] \\ r_2 \sin[2\pi(k-4)/3 + \alpha] \\ H \end{bmatrix} \quad (k=4, 5, 6) \quad (3)$$

Since an additional node must be located inside the triangle enclosed by the existing nodes, coordinates of the additional nodes can be defined by coordinates of the existing nodes with the barycentric coordinates. Expressions for calculating coordinates of the additional nodes depend on connectivity of the additional strings. In Type 1, coordinates of the three additional nodes can be written as

$$\begin{aligned} N_7 &= c_1 N_6 + c_2 N_4 + (1 - c_1 - c_2) N_3 \\ N_8 &= c_1 N_5 + c_2 N_6 + (1 - c_1 - c_2) N_2 \\ N_9 &= c_1 N_4 + c_2 N_5 + (1 - c_1 - c_2) N_1 \end{aligned} \quad (4)$$

where $c_1, c_2, (c_1 + c_2) \in (0, 1)$.

When r_1, r_2, H, c_1, c_2 and α are given, nodal coordinates can be calculated easily. However, arbitrary assignments of these parameters might not result in a self-equilibrated configuration.

4 Analytical Solutions

In this section, we present the analytical conditions for self-equilibrium of the three new tensegrity units consisting of additional nodes and strings. Self-equilibrium of a tensegrity is decided by its nodal locations as well as the combination of internal forces in all the members. There are six kinds of members in the tensegrity units investigated in this paper. The members of the same kind are assumed to have the same length and internal forces according to symmetry; i.e., there are six different force densities in the structures. Since there are three types of nodes, which are the nodes on the lower plane, the nodes on the upper plane and the additional nodes, we can establish nine independent equilibrium equations, three equations for each type of nodes. Symbolic computation software package Maple 2016 [19] is used for assisting derivation of analytical solutions.

4.1 Type 1

For Type 1, set up the local coordinate system as shown in Fig.3. Four nodes are located on (\bar{x}, \bar{y}) plane in the local coordinate system, and nodes 1 and 5 are located on the \bar{x} axis.

Because relative location of the nodes in two coordinate systems as shown in Figs.1 and 3 are not changed, coordinates of additional node 9 in local coordinate system can be also written as

$$\begin{cases} \bar{x}_9 = c_1 \bar{x}_4 + c_2 \bar{x}_5 + (1 - c_1 - c_2) \bar{x}_1 \\ \bar{y}_9 = c_1 \bar{y}_4 + c_2 \bar{y}_5 + (1 - c_1 - c_2) \bar{y}_1 \end{cases} \quad (5)$$

Rearranging Eq.(5), while \bar{x}_1 , \bar{y}_1 and \bar{y}_5 are all equal to 0, we have

$$\begin{cases} \bar{x}_9 = c_1 \bar{x}_4 + c_2 \bar{x}_5 \\ \bar{y}_9 = c_1 \bar{y}_4 \end{cases} \quad (6)$$

Using the standard formulation of force density method, the equilibrium equations of node 9 on (\bar{x}, \bar{y}) plane can be written as follows:

$$\begin{cases} (\bar{x}_5 - \bar{x}_9) \gamma_{ul1} + (\bar{x}_4 - \bar{x}_9) \gamma_{ul2} - \bar{x}_9 \gamma_a = 0 \\ -\bar{y}_9 \gamma_{ul1} + (\bar{y}_4 - \bar{y}_9) \gamma_{ul2} - \bar{y}_9 \gamma_a = 0 \end{cases} \quad (7)$$

where γ_a , γ_{ul1} and γ_{ul2} are the force densities of the additional strings, the first and second upper level strings, respectively.

Substituting Eq.(6) into Eq.(7), we have

$$\begin{cases} (\gamma_{ul1} - c_2 \gamma_{ul1} - c_2 \gamma_{ul2} - c_2 \gamma_a) \bar{x}_5 + (-c_1 \gamma_{ul1} + \gamma_{ul2} - c_1 \gamma_{ul2} - c_1 \gamma_a) \bar{x}_4 = 0 \\ -c_1 \gamma_{ul1} + (1 - c_1) \gamma_{ul2} - c_1 \gamma_a = 0 \end{cases} \quad (8)$$

In Eq.(8), the left-hand side of second equation is the same as coefficient of \bar{x}_4 in the first equation. So Eq.(8) can be simplified into

$$\begin{cases} \gamma_{ul1} - c_2 \gamma_{ul1} - c_2 \gamma_{ul2} - c_2 \gamma_a = 0 \\ -c_1 \gamma_{ul1} + (1 - c_1) \gamma_{ul2} - c_1 \gamma_a = 0 \end{cases} \quad (9)$$

From Eq.(9), γ_{ul1} and γ_{ul2} can be expressed as

$$\begin{aligned}\gamma_{ul1} &= \frac{\gamma_a c_1}{1 - c_2 - c_1} \\ \gamma_{ul2} &= \frac{\gamma_a c_2}{1 - c_2 - c_1}\end{aligned}\quad (10)$$

Using the global coordinate system, equilibrium equations of nodes 1 and 6 can be written as

$$\begin{cases} (x_1 - x_4)\lambda + (x_6 - x_1)\gamma_v + (x_2 + x_3 - 2x_1)\gamma_{bl} + (x_9 - x_1)\gamma_a = 0 \\ (y_1 - y_4)\lambda + (y_6 - y_1)\gamma_v + (y_2 + y_3 - 2y_1)\gamma_{bl} + (y_9 - y_1)\gamma_a = 0 \\ (z_1 - z_4)\lambda + (z_6 - z_1)\gamma_v + (z_2 + z_3 - 2z_1)\gamma_{bl} + (z_9 - z_1)\gamma_a = 0 \\ (x_6 - x_3)\lambda + (x_1 - x_6)\gamma_v + (x_8 - x_6)\gamma_{ul1} + (x_7 - x_6)\gamma_{ul2} = 0 \\ (y_6 - y_3)\lambda + (y_1 - y_6)\gamma_v + (y_8 - y_6)\gamma_{ul1} + (y_7 - y_6)\gamma_{ul2} = 0 \\ (z_6 - z_3)\lambda + (z_1 - z_6)\gamma_v + (z_8 - z_6)\gamma_{ul1} + (z_7 - z_6)\gamma_{ul2} = 0 \end{cases}\quad (11)$$

where λ , γ_v and γ_{bl} are the force densities of bars, declining strings and lower level strings, respectively. After substituting Eqs.(2), (3), (4) and (10) into Eq.(11) and solving it, we can obtain

$$c_2 = (\sqrt{3} \sin \alpha + \cos \alpha) \frac{c_1 r_2}{r_1} - c_1 + 1 \quad (12)$$

Other force densities can be also obtained as

$$\begin{aligned}\lambda &= \frac{\gamma_a [-\sqrt{3}c_1 r_2 \sin(2\alpha) + c_1 r_2 \sin^2 \alpha - \sqrt{3}c_1 r_1 \sin \alpha - c_1 r_2 \cos^2 \alpha + c_1 r_1 \cos \alpha - 2r_1 \cos \alpha - c_1 r_2]}{r_1 (\sqrt{3} \sin \alpha + \cos \alpha)} \\ \gamma_v &= -\frac{\gamma_a (-\sqrt{3}c_1 r_1 \sin \alpha + 4c_1 r_2 \sin^2 \alpha + c_1 r_1 \cos \alpha + \sqrt{3}r_1 \sin \alpha - r_1 \cos \alpha - c_1 r_2)}{r_1 (\sqrt{3} \sin \alpha + \cos \alpha)} \\ \gamma_{bl} &= -\frac{\gamma_a r_2 (\sqrt{3}c_1 r_2 \sin \alpha + c_1 r_2 \cos \alpha + r_1 - c_1 r_1)}{r_1^2 (\sqrt{3} \sin \alpha + \cos \alpha)}\end{aligned}\quad (13)$$

As presented in Eq.(4), $(1 - c_1 - c_2)$ must be greater than 0, namely, from Eq.(12), we have

$$(\sqrt{3} \sin \alpha + \cos \alpha) \frac{c_1 r_2}{r_1} > 0 \quad (14)$$

From Eq.(14), we have

$$\tan \alpha > -\frac{\sqrt{3}}{3} \quad (15)$$

Namely, α must be greater than 150° .

4.2 Type 2

For Type 2, we can obtain the same results as Eq.(10) through equilibrium equations at the additional node. In Type 2, equilibrium equations at nodes 1 and 6 can be written as

$$\text{Node 1} \begin{cases} (x_1 - x_4)\lambda + (x_6 - x_1)\gamma_v + (x_2 + x_3 - 2x_1)\gamma_{bl} + (x_9 - x_1)\gamma_a = 0 \\ (y_1 - y_4)\lambda + (y_6 - y_1)\gamma_v + (y_2 + y_3 - 2y_1)\gamma_{bl} + (y_9 - y_1)\gamma_a = 0 \\ (z_1 - z_4)\lambda + (z_6 - z_1)\gamma_v + (z_2 + z_3 - 2z_1)\gamma_{bl} + (z_9 - z_1)\gamma_a = 0 \end{cases}\quad (16)$$

$$\text{Node 6} \begin{cases} (x_6 - x_3)\lambda + (x_1 - x_6)\gamma_v + (x_7 - x_6)\gamma_{ul1} + (x_9 - x_6)\gamma_{ul2} = 0 \\ (y_6 - y_3)\lambda + (y_1 - y_6)\gamma_v + (y_7 - y_6)\gamma_{ul1} + (y_9 - y_6)\gamma_{ul2} = 0 \\ (z_6 - z_3)\lambda + (z_1 - z_6)\gamma_v + (z_7 - z_6)\gamma_{ul1} + (z_9 - z_6)\gamma_{ul2} = 0 \end{cases}$$

After substituting node coordinates into Eq.(16), we have

$$\begin{cases} (k_1 + 2\gamma_{bl} + 2\gamma_a)r_1 + \gamma_{bl}r_1 - \lambda r_2 \cos \alpha - \gamma_v k_2 - \gamma_a(c_1 k_2 + c_2 r_2 \cos \alpha - k_3 r_1) = 0 \\ -\lambda r_2 \sin \alpha - \gamma_v k_4 - \gamma_a(c_1 k_4 + c_2 r_2 \sin \alpha) = 0 \\ -\lambda h - \gamma_v h - \gamma_a(c_1 + c_2)h = 0 \\ \frac{1}{k_3} [k_3 \cos \alpha + \frac{1}{2} c_1^2 \gamma_a r_1 + k_6 c_1 - \gamma_a c_2^2 r_1 + (\gamma_a - \lambda + \frac{1}{2} \gamma_v) r_1 c_2 + (\lambda - \frac{1}{2} \gamma_v) r_1] = 0 \\ \frac{1}{k_3} \{ [c_1^2 \gamma_a + (k_1 - \gamma_a c_2) c_1 + \gamma_a c_2^2 + k_1 c_2 - \lambda - \gamma_v] r_2 \sin \alpha - \frac{\sqrt{3}}{2} c_1^2 \gamma_a r_1 + k_7 \} = 0 \\ h[(c_1 + c_2)\gamma_a + \lambda + \gamma_v] = 0 \end{cases} \quad (17)$$

where

$$\begin{aligned} k_1 &= \lambda + \gamma_v - \gamma_a \\ k_2 &= -\frac{1}{2} r_2 \cos \alpha + \frac{\sqrt{3}}{2} r_2 \sin \alpha \\ k_3 &= c_1 + c_2 - 1 \\ k_4 &= -\frac{\sqrt{3}}{2} r_2 \cos \alpha - \frac{1}{2} r_2 \sin \alpha \\ k_5 &= c_1^2 \gamma_a r_2 - \gamma_a c_2 r_2 - \gamma_a c_2 r_2 c_1 + k_1 r_2 (c_1 + c_2) + \gamma_a c_2^2 r_2 - \lambda r_2 - \gamma_v r_2 \\ k_6 &= -\frac{1}{2} \gamma_a c_2 r_1 - \lambda r_1 + \frac{1}{2} \gamma_v r_1 - \frac{1}{2} \gamma_a r_1 \\ k_7 &= -\frac{\sqrt{3}}{2} c_1 \gamma_v r_1 - \frac{\sqrt{3}}{2} \gamma_a c_1 c_2 r_1 + \frac{\sqrt{3}}{2} c_1 r_1 \gamma_a - \frac{\sqrt{3}}{2} \gamma_v r_1 c_2 + \frac{\sqrt{3}}{2} \gamma_v r_1 \end{aligned}$$

From the sixth equation in Eq.(17), the force density of strut is written as

$$\lambda = -c_1 \gamma_a - c_2 \gamma_a - \gamma_v \quad (18)$$

After substituting Eq.(18) to the second equation of Eq.(17), we obtain

$$(\gamma_v + \gamma_a c_1)(\sin \alpha + \sin(\alpha + \frac{\pi}{3})) = 0 \quad (19)$$

From Eq.(19), we find that either of the following equations is satisfied:

$$\begin{cases} \gamma_v = -c_1 \gamma_a \\ \sin \alpha + \sin(\alpha + \frac{\pi}{3}) = 0 \Rightarrow \alpha = 150^\circ \end{cases} \quad (20)$$

Since γ_v and γ_a are force densities which must be positive, the first expression of Eq.(20)

is not correct. Therefore α should be equal to 150° in Type 2.

4.3 Type 3

In Type 3 as shown in Fig.2(c), nodes 1, 5, 6 and 9 are located on the same plane. We can also set up equations similar to Eqs.(5)-(8), and can obtain the same results as Eq.(10). Nodes 1 and 6 are chosen to set up equilibrium equations similar to Eq.(11). Process for solving other parameters is also the same as Type 1. So analysis for Type 3 is almost the same as Type

1 and is not described in detail here. In Type 3, we can obtain

$$c_1 = (\sqrt{3} \sin \alpha + \cos \alpha) \frac{c_2 r_2}{r_1} - c_2 + 1 \quad (21)$$

Difference between Eqs.(12) and (21) is only that c_1 and c_2 exchange places with each other. Force densities of the members can be expressed as

$$\begin{aligned} \lambda &= \frac{\gamma_a [-\sqrt{3}c_2 r_2 \sin(2\alpha) + c_2 r_2 \sin^2 \alpha - c_2 r_2 \cos^2 \alpha + 2c_2 r_1 \cos \alpha - 2r_1 \cos \alpha - c_2 r_2]}{r_1 (\sqrt{3} \sin \alpha + \cos \alpha)} \\ \gamma_v &= -\frac{\gamma_a (4c_2 r_2 \sin^2 \alpha + \sqrt{3}r_1 \sin \alpha + 2c_2 r_1 \cos \alpha - r_1 \cos \alpha - c_2 r_2)}{r_1 (\sqrt{3} \sin \alpha + \cos \alpha)} \\ \gamma_{bt} &= -\frac{\gamma_a r_2 (\sqrt{3}c_2 r_2 \sin \alpha + c_2 r_2 \cos \alpha + r_1 - c_2 r_1)}{r_1^2 (\sqrt{3} \sin \alpha + \cos \alpha)} \\ \gamma_{ul1} &= \frac{\gamma_a c_1}{1 - c_2 - c_1} \\ \gamma_{ul2} &= \frac{\gamma_a c_2}{1 - c_2 - c_1} \end{aligned} \quad (22)$$

5 Investigation of Analytical Solutions

5.1 Type 1

It is well known that the equilibrium equation with respect to the force densities is invariant with respect to affine transformation of nodal coordinates [21]. Therefore, some geometrical parameters can be assigned without loss of generality. Hence, in the following numerical examples, H is assigned as 0.25m, and r_1 is 0.1m. Since the force densities of members can be simultaneously scaled, we assign $\gamma_a = 1$. The parameter $k = r_2 / r_1$ is used in the following investigation.

Based on Eq.(12), c_2 and $(1-c_1-c_2)$ are plotted with respect to c_1 and α ($\geq 150^\circ$) in Fig. 4, where $r_2 = r_1$ ($k = 1$), and surfaces 1 and 2 show c_2 and $(1-c_1-c_2)$, respectively. As seen in the figure, with increase of α , c_2 decreases and $(1-c_1-c_2)$ increases; with increase of c_1 , c_2 decreases and $(1-c_1-c_2)$ increases. When c_1 is equal to 0, c_2 is always equal to 1 and $(1-c_1-c_2)$ is always equal to 0; namely the first and second upper level strings are on the same lines, which means that the added nodes 7, 8 and 9 cannot be at equilibrium and the structures are not self-equilibrated. Furthermore, if α is equal to 150° , then $(1-c_1-c_2)$ is equal to 0. When α is greater than 150° , $(1-c_1-c_2)$ is always greater than 0. So α should be greater than 150° , which is the same as conclusion obtained from Eq.(15).

It is seen from Fig.4 that the range of c_1 decreases with increase of α . When c_2 is equal to 0, c_1 reaches the following maximal value c_1^{\max} as a function of α and k :

$$c_1^{\max} = \frac{1}{1 - k(\sqrt{3} \sin \alpha + \cos \alpha)} \quad (23)$$

Therefore, the range of c_1 is found as $c_1 \in (0, [1 - k(\sqrt{3} \sin \alpha + \cos \alpha)]^{-1})$. It is also observed from Fig.4 that the maximum value of c_1 is always greater than or equal to 0.5. Moreover, the greater c_1 is, the more obvious influence α has on c_2 .

The relation in Fig.4 also depends on the parameter $k = r_2 / r_1$. So assign c_1 as 0.4 here to investigate influence of α and k on c_2 . Curved surfaces 1 and 2 in Fig.5 are the plots of c_2 and c_1^{\max} , respectively, with respect to k and α . As seen from surfaces 1 and 2, with increase of k , both of c_2 and c_1^{\max} decrease. With increase of α , the two values also decreases.

As discussed by Zhang and Ohsaki [16], there are always at least four zero eigenvalues in the force density matrix of the self-equilibrated structures. This condition is called self-equilibrium conditions here. Substituting 0.1 to r_1 and r_2 ($k = 1$) in Eq. (12), we obtain

$$c_2 = c_1(\cos \alpha + \sqrt{3} \sin \alpha) - c_1 + 1 \quad (24)$$

Then suppose c_1 can vary in the range $(0, (1 - \sqrt{3} \sin \alpha - \cos \alpha)^{-1})$, and obtain some groups of node coordinates in Type 1.

Figure 6 shows the structures in Type 1 when $\alpha > 150^\circ$. It is seen from Eq.(24) that c_2 is a linear function of c_1 when α is given *a priori*. With variation of c_1 in the range $(0, (1 - \sqrt{3} \sin \alpha - \cos \alpha)^{-1})$, each additional node moves along a line, as shown in Fig. 6, on the triangle that is defined by three existing nodes and enclose the additional node. We confirmed that the self-equilibrium conditions in reference [16] are always satisfied. When value of c_1 is not in its range, the additional nodes will move outside of the triangles, and internal forces of the members connected to the additional nodes cannot keep the nodes at equilibrium, so the structure is not self-equilibrated. Moreover, there will appear negative eigenvalues of the force density matrix and the structure is not super-stable.

Figure 7 shows a physical model of Type 1. It is self-equilibrated with $\alpha = 175^\circ$. As seen in Fig. 7(b), the bars are close to each other, but they do not physically contact; however, because the bars and additional strings are all located inside of the cylinder, interferences among the members easily occur.

An example with $\alpha < 150^\circ$ of Type 1 is shown in Fig.8. Although the additional nodes are still located on the corresponding lines, they have moved out of the triangles which enclose them. Three strings connected at every additional node can't keep the additional node at equilibrium. Therefore, α must be greater than 150° so that the structure is at self-equilibrium. This fact is similar to conclusion from Eq.(15).

5.2 Type 2

As presented in Section 4.2, α should be equal to 150° in Type 2. We investigate six equations in Eq.(17), which are the equilibrium equations of nodes 1 and 6. Since γ_{bl} exists only in the first equation of Eq.(17), it can be solved to obtain γ_{bl} . From the sixth equation in Eq.(17), the force density of bar can be expressed as Eq.(18). It is difficult to derive expressions of c_1 and c_2 with symbolic form of γ_a , and the expressions can be obtained only when γ_a is given. For example, when γ_a is equal to 1.4, after substituting Eq.(18) and

$\alpha=150^\circ$ to the fifth equation of Eq.(17) and solving it, we can obtain

$$\gamma_v = \frac{c_1(1.4c_1 + 3.825c_2 - 1.4)}{1 - c_1 - c_2} \quad (25)$$

After substituting Eq.(25) into the fourth equation of Eq.(17), c_2 can be solved as

$$c_2 = \frac{c_1(0.596c_1 - 1.809)}{1 - 1.057c_1} \quad (26)$$

The second and third equations of Eq.(17) are linearly related to the sixth equation of Eq.(17); so all force densities and nodal locations are determined by assigning γ_a and c_1 .

So relation between c_1 and c_2 depends on γ_a , and different γ_a results in different location of the additional node. When an arbitrary positive force density is assigned to the additional strings, the additional nodes are always located in the triangles which enclose them; namely, only if the additional strings are in the triangles which enclose them, the structure can satisfy the self-equilibrium condition and is at self-equilibrium.

5.3 Type 3

Because Eq.(21) can be obtained by exchanging c_1 and c_2 in Eq.(12), conclusions from Eq.(12) can be also applicable to Type 3; i.e., α should be greater than 150° ; c_1 is a decreasing function of both α and c_2 ; and c_2 reaches the following maximal value c_2^{\max} when c_1 is equal to 0:

$$c_2^{\max} = \frac{1}{1 - k(\sqrt{3} \sin \alpha + \cos \alpha)} \quad (27)$$

Hence, $c_2 \in (0, [1 - k(\sqrt{3} \sin \alpha + \cos \alpha)]^{-1})$. In the similar manner as Section 5.1, c_2^{\max} is an decreasing function of k and α .

Figure 9 shows an example of geometry realization of the Type 3 structure. As seen in Fig.9, each additional node moves along a line as c_2 is varied; namely, as long as the additional nodes are on the lines within the corresponding triangles, the self-equilibrium condition is always satisfied. When c_2 is outside of its range, the additional nodes move out of the triangles and equilibrium conditions are not satisfied with tensile forces in strings; accordingly, there are negative eigenvalues of the force density matrix and the structure is not stable. Figure 10 shows the Type 3 structure with $\alpha=170^\circ$, which confirms that the Type 3 structure can be self-equilibrated when α is greater than 150° .

When $\alpha < 150^\circ$, the additional nodes move out of the triangles which enclose them, as shown in Fig.11; hence, the structure in Fig.11 is not at self-equilibrium. So in Type 3, α should be greater than 150° .

6 Numerical Investigation of Internal Forces

Detailed investigations of internal forces are given in this section for Type 1 and 3 structures. Type 2 is excluded, because it allows only limited shape with $\alpha = 150^\circ$.

6.1 Type 1

Based on the expressions (10) and (13) for force densities of Type 1 structure, we will analyze relations between internal forces of the members and other parameters. In Figs. 12-15, the vertical axis refers to ratio of internal forces of each member to the force of additional string. We found in Figs. 4 and 5 in Section 5 that the maximum value of c_1 is always greater than 0.5. Moreover, when c_1 is equal to its maximal value, c_2 is equal to 0; when c_1 is equal to 0, c_2 is equal to 1. So we assign an intermediate value 0.3 to c_1 . Figure 12 shows the values of internal forces with respect to α . Here let $f_b, f_v, f_{bl}, f_a, f_{ul1}$ and f_{ul2} represent internal forces of the bars, declining strings, lower level strings, additional strings, the first and second upper level strings, respectively.

It is seen from Fig. 12 that, with increase of α , f_a is almost constant and absolute values of other internal forces decrease. Distribution of the internal force is uneven as α is close to 150° . When α is equal to 150° , f_v and f_{ul2} tend to infinity. So α cannot be equal to 150° .

When α is equal to 180° , ratio of the maximal force to the minimal force of string reaches 50 and distribution of the internal force is also uneven.

When α is about 165° , distribution of the internal force is most even. So we set $\alpha = 165^\circ$ to analyze influence of c_1 on internal forces. Figure 13 shows variations of internal forces of the members with respect to c_1 . As seen in Fig. 13, with increase of c_1 , f_{ul1} increases, f_a is almost constant and absolute values of other forces all decrease.

In Type 1, node 9 connected to node 1 is supported by the two upper level strings connecting node 9 to nodes 4 and 5. With increase of c_1 , node 9 moves from node 4 to 5. When c_1 becomes close to 0, namely, node 9 approaches to node 4, there is apparent uneven distribution of internal forces. When c_1 approaches its maximal value, node 9 moves toward node 5, and f_{bl}, f_v and f_{ul2} are all equal to 0 resulting in uneven distribution of internal forces. So when additional nodes are not close to any existing node, the internal forces are distributed more evenly.

6.2 Type 3

Using expressions (22) of force densities in Type 3, influences of other parameters on internal forces are investigated. Figure 14 shows variations of internal forces with respect to c_2 in Type 3 when $\alpha = 165^\circ$. As seen in Fig. 14, with increasing of c_2 , f_{ul2} increases, f_a is almost constant, and absolute values of other forces all decrease. In Type 3, node 9 connected to node 1 is located to the first and second upper level strings connecting node 9 to nodes 5 and 6, respectively. When c_1 increases, node 9 moves toward node 5. Conversely, node 9 approaches to node 6. When node 9 becomes close to node 6, i.e., $c_1 = 1$, f_{ul1} will increase rapidly to 52.23, while

absolute values of all other forces are below 5. When c_2 becomes larger and node 9 approaches to node 5, f_b , f_{bl} and f_{ul} decrease to 0. So when additional nodes approach the existing nodes, uneven distribution of the internal forces becomes apparent. This is the same as Type 1. Moreover, when c_2 is beyond 0.53, f_v becomes negative and equilibrium conditions are not satisfied with positive forces in strings; i.e., the structure is not stable.

Internal forces when $c_1=0.3$ are plotted with respect to α in Fig.15, which shows that with increase of α , f_a is almost constant and absolute values of all other force densities decrease. When α approaches to 150° or 180° , difference among the internal forces becomes large. This is the same as observed in Type 1.

Through the above numerical analysis, we can obtain the following conclusions for Types 1 and 3 structures:

- 1) Distribution of the internal forces becomes uneven as the additional nodes approach to existing nodes.
- 2) When α approaches to 150° or 180° , there are apparent uneven distribution of the internal forces.

When $\alpha=150^\circ$, the 3-bar prismatic tensegrity unit without additional strings is self-equilibrated. For Types 1 and 3, distribution of internal forces and the value of α change as the forces of the additional strings are increased. Moreover, the structure is self-equilibrated if additional nodes are in the triangles which enclose them. If we allow uneven distribution of internal forces, the range of α should be $[150^\circ, 180^\circ]$ in Types 1 and 3.

In Type 2, it is difficult to obtain general expressions of force densities, because relation between c_1 and c_2 depends on γ_a . Relations between internal forces of the members and other parameters are difficult to be investigated.

Because it has been presented that the two 3-bar tensegrity units when $\alpha=150^\circ$ and -150° are symmetrical, we can deduce easily characteristics of new configurations when $\alpha=-150^\circ$ from conclusions of $\alpha=150^\circ$. So analysis for new configurations when $\alpha=-150^\circ$ is not described here.

7 Conclusions

In the paper, we presented three new types of tensegrity units by adding strings and nodes to the well-known 3-bar prismatic tensegrity unit. The strings are added between the nodes on the lower plane and the level strings on the upper plane. The three types are characterized by the connectivity of the additional string to the additional nodes located on the upper level strings.

Type 1 and 3 structures have the following characteristics:

- (1) Additional node 9 connected to node 1 should be located between nodes 4 and 5 or 5 and 6. The tensegrity units when $\alpha > 0$ are always self-equilibrated when $\alpha \in [150^\circ, 180^\circ]$. The tensegrity units when $\alpha < 0$ are always at self-equilibrium when $\alpha \in [-180^\circ, -150^\circ]$.
- (2) The additional nodes are located on the lines which are obtained through analysis in Sections 4 and 5. Moreover they must stay in the triangles which enclose them.
- (3) As the additional nodes approach to existing nodes, distribution of the internal forces becomes uneven; conversely, distribution of the internal forces becomes uniform if the additional node is sufficiently apart from the existing nodes.
- (4) When α approaches to $\pm 150^\circ$ or $\pm 180^\circ$, there are apparent uneven distribution of the internal forces.

Type 2 structure can maintain self-equilibrated only when $\alpha = \pm 150^\circ$. Since the equilibrium shape is strongly limited, we did not investigate details of Type 2 structure.

Acknowledgment

The authors gratefully acknowledge the contribution of National Natural Science Fund of China (Grant Number 51605111, 51675114) and JSPS KAKENHI (Grant Number 15KT0109).

Reference

- [1] R. Motro, L. Jia and B. Yang. Tensegrity—From art to structure engineering. *Building Structures* 2011;12:12-19.
- [2] J. Cai and J. Feng. From-finding of tensegrity structures using an optimization method. *Engineering Structures*, 2015; 104:26-132.
- [3] C. Sultan. Tensegrity: 60 years of art, science, and engineering. *Advances in applied mechanics* 2009;43:69-145.
- [4] A. Agogino, V. SunSpiral and D. Atkinson. Super Ball Bot-Structures for Planetary Landing and Exploration. NASA Innovative Advanced Concepts (NIAC) Program 2013(7).
- [5] A. Amendola, E.H. Nava, R. Goodall, I. Todd, R.E. Skelton and F. Fraternali. On the additive manufacturing, post-tensioning and testing of bi-material tensegrity structures. *Composite Structures* 2015;131:66-71.
- [6] N. Ashwear, G. Tamadapu and A. Eriksson. Optimization of modular tensegrity structures for high stiffness and frequency separation requirements. *International Journal of Solids and Structures*, 2016; 80:297–309.
- [7] Y. Koizumi, M. Shibata and S. Hirai. Rolling tensegrity driven by pneumatic soft actuators. In: 2012 IEEE International Conference on Robotics and Automation, RiverCentre, Minnesota, USA; 2012:1988-1993.
- [8] W. Du, S. Ma, B. Li, M. Wang and S. Hirai. Dynamic simulation for 6-strut tensegrity robots. In: Proceeding of the IEEE International Conference on Information and Automation, Hailar, China;2014: 870-875.

- [9] S. Hirai and R. Imuta. Dynamic simulation of six-strut tensegrity robot rolling. In: Proceedings of the 2012 IEEE International Conference on Robotics and Biomimetics, Guangzhou, China;2012: 198-204.
- [10] K. Caluwaerts and J.P. Carbajal. Energy conserving constant shape optimization of tensegrity structures. *International Journal of Solids and Structures* 2015;58:117-127.
- [11] H. Liu, J. Geng and A. Luo. Tensegrity configuration method on connecting tensegrity units along their axes. *Composite Structure* 2017;162:341-350.
- [12] A. Luo, Q. Li, H. Liu, J. Cheng and L. Xu. Establishment and mechanical properties analysis of spherical tensegrity structures. In: 5th Structural Engineers World Congress(SEWC 2015), Singapore; 2015:19-22.
- [13] S. Pellegrino. Structural computations with the singular value decomposition of the equilibrium matrix. *International Journal of Solids and Structures* 1993;30(21): 3025-3035.
- [14] P. Zhang and J. Feng. Initial prestress design and optimization of tensegrity systems based on symmetry and stiffness. *International Journal of Solid and Structures* 2017;106:68-90.
- [15] X. Xu, S. Li and Y. Luo. Form-finding of a new kind of tensegrity tori using overlapping modules. *Mechanics Research Communications* 2017;84:1-7.
- [16] J. Y. Zhang and M. Ohsaki. *Tensegrity Structures: Form, Stability, and Symmetry*. Springer;2015.
- [17] A.G. Tibert and S. Pellegrino. Review of form-finding methods for tensegrity structures. *International Journal of Space Structures* 1986;26(3):241-255.
- [18] M. Schenk, J.L. Herder and S.D. Guest. Design of a statically balanced tensegrity mechanism. In: ASME 2006 International Design Engineering Technical Conferences & Computers and Information in Engineering Conference, Pennsylvania, USA; 2006:10-13.
- [19] P. Zhang, K. Kawaguchi and J. Feng. Prismatic tensegrity structures with additional cables: Integral symmetric states of self-stress and cable-controlled reconfiguration procedure. *International Journal of Solids and Structures* 2014;51:4294-4306.
- [20] Maplesoft, *Maple 2016 User Manual*, 2016.
- [21] J. Y. Zhang and M. Ohsaki. Stability conditions for tensegrity structures. *International Journal of Solids and Structures* 2007;44(11-12):3875-3886.

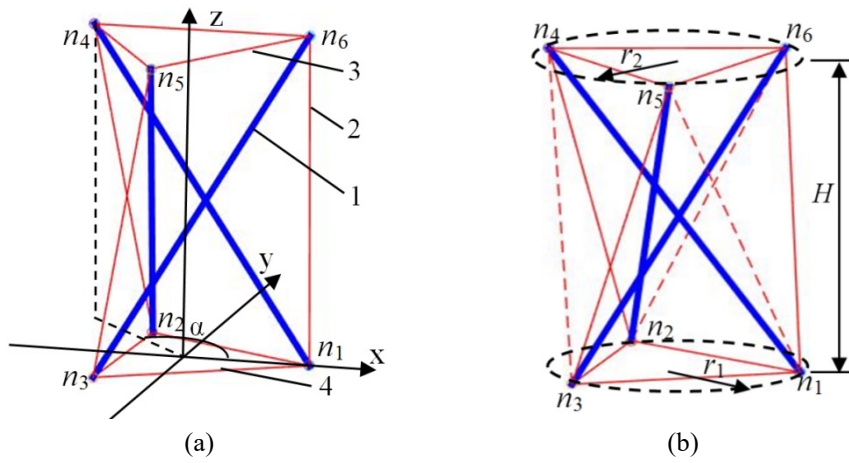


Fig.1 3-bar prismatic tensegrity unit and its configuration; 1: bar, 2: declining string, 3: upper level string, 4: lower level string

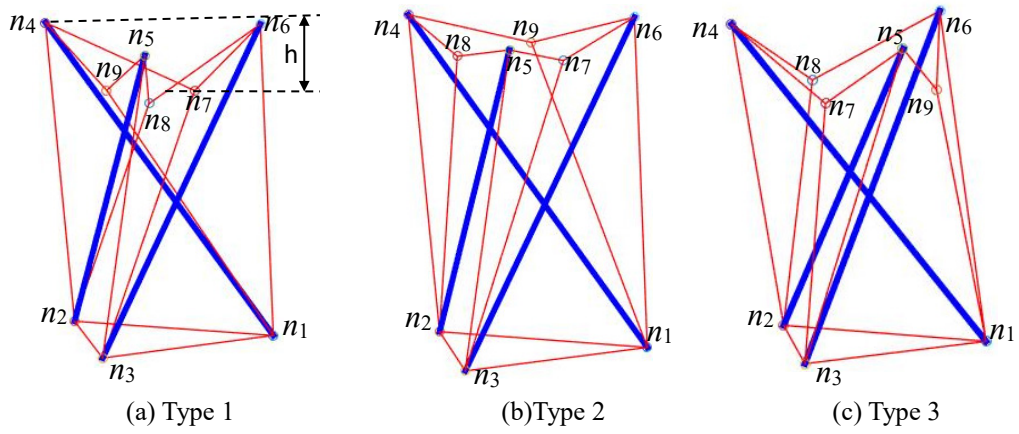


Fig.2 Three types of 3-bar prismatic tensegrity units with the additional nodes and strings

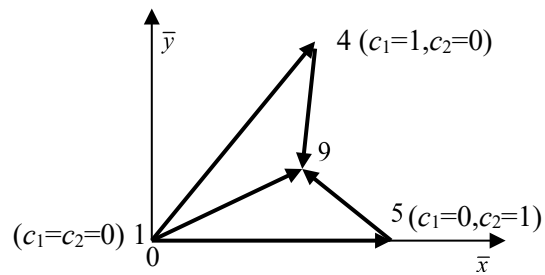


Fig.3 Nodes 1, 4, 5 and 9 in local coordinate system

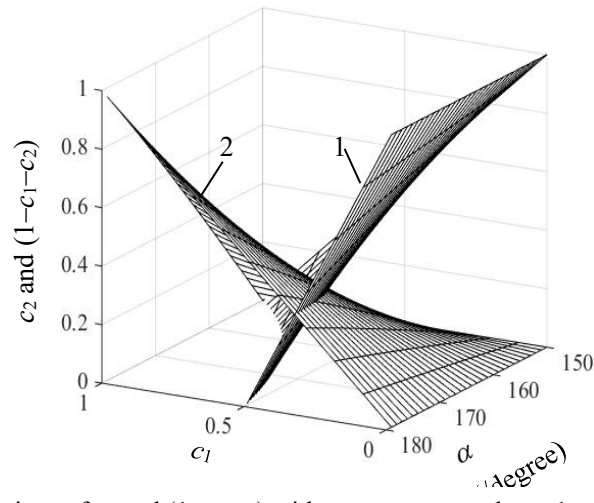


Fig.4 Variations of c_2 and $(1-c_1-c_2)$ with respect to c_1 and α ; 1: c_2 , 2: $(1-c_1-c_2)$

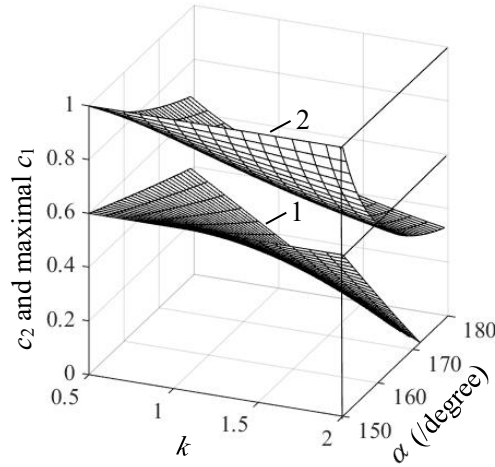


Fig.5 Variations of c_2 and c_1^{\max} with respect to k and α ; 1: c_2 , 2: c_1^{\max}

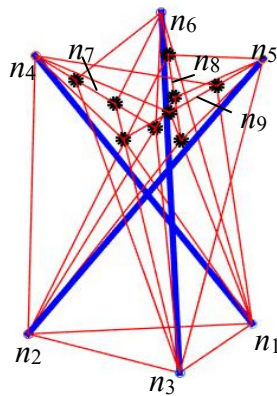
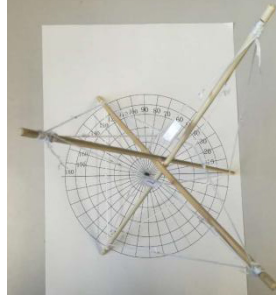
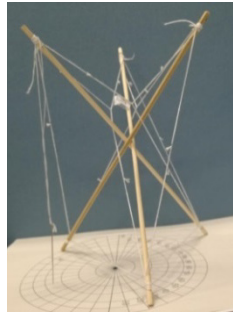


Fig.6 Analysis results in Type1 when $\alpha > 150^\circ$



(a) Model

(b) Top view

Fig.7 A self-equilibrated configuration of Type 1

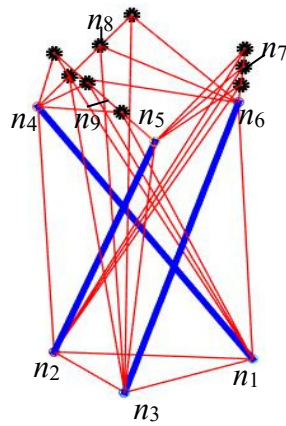


Fig.8 Analysis results of Type1 when $\alpha < 150^\circ$

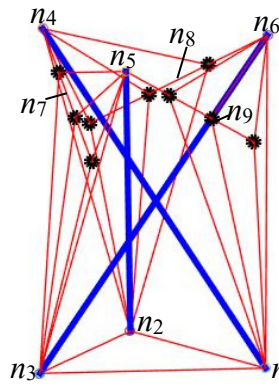
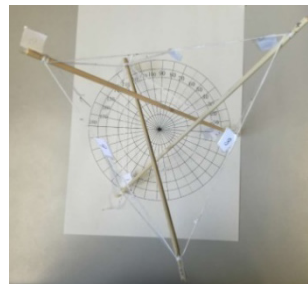


Fig.9 An example structure of Type 3 with $\alpha \geq 150^\circ$



(a) Model

(b) Top view

Fig.10 A Physical model of Type 3

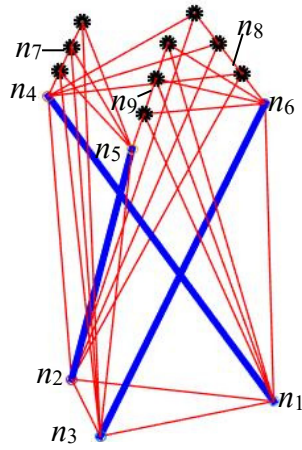


Fig.11 Analysis results in Type3 when $\alpha < 150^\circ$

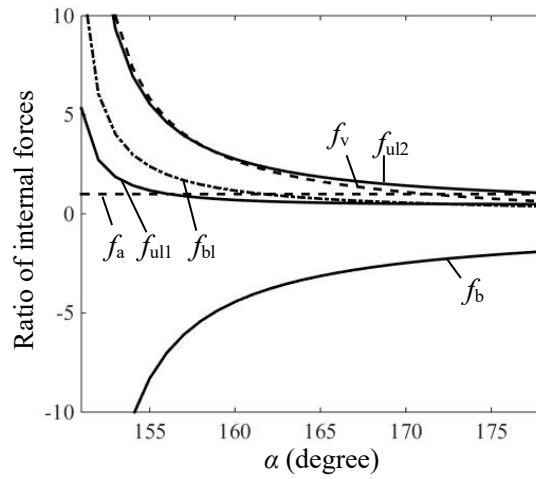


Fig.12 Variations of internal forces with respect to α of Type 1 structure with $c_1=0.3$

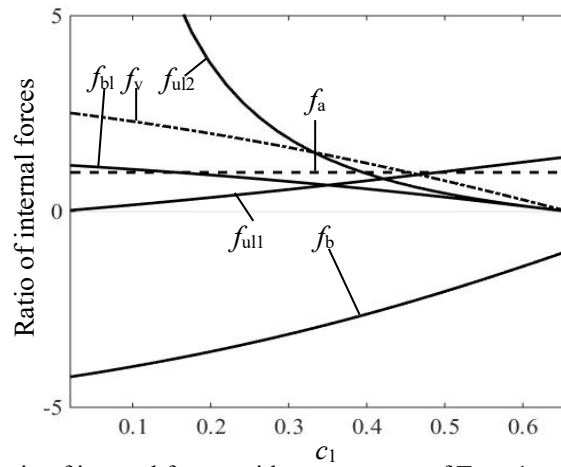


Fig.13 Variations of ratio of internal forces with respect to c_1 of Type 1 structure with $\alpha=165^\circ$

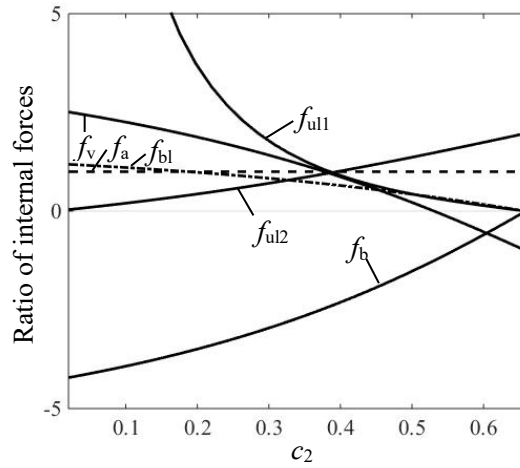


Fig.14 Variations of ratio of internal forces with respect to c_2 of Type 3 structure with $\alpha=165^\circ$

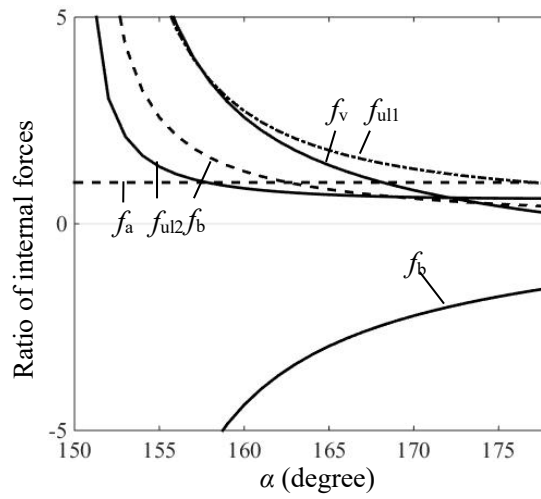


Fig.15 Curves of ratio of internal forces with respect to α in Type 3 with $c_2=0.3$

Table 1 Node groups of Types 1, 2 and 3

Type	Node group
Type 1 in Fig.2(a)	{1,9,4,5}, {3,7,6,4}, {2,8,5,6}
Type 2 in Fig.2(b)	{1,9,6,4}, {3,7,5,6}, {2,8,4,5}
Type 3 in Fig.2(c)	{1,9,5,6}, {3,7,4,5}, {2,8,6,4}